QUARTERLY JOURNAL OF THE ROYAL METEOROLOGICAL SOCIETY
Q. J. R. Meteorol. Soc. (2010)
Published online in Wiley InterScience
(www.interscience.wiley.com) DOI: 10.1002/qj.554

RMetS
Royal Meteorological Society

Intraseasonal variability of the ocean – atmosphere coupling in the Gulf of Guinea during boreal spring and summer

Gaëlle de Coëtlogon,[a]* Serge Janicot[b] and Alban Lazar[b]
[a]*LATMOS–IPSL, Université Pierre et Marie Curie, Paris, France*
[b]*LOCEAN–IPSL, Université Pierre et Marie Curie, Paris, France*

ABSTRACT: Statistical analyses of the satellite TMI sea-surface temperature (SST) and QuikSCAT surface winds in boreal spring and summer are performed to investigate the intraseasonal variability of air–sea interactions in the Gulf of Guinea. There, empirical orthogonal function decomposition shows the existence of peaks around 15 days, and their lagged cross-correlation the signature of an expected 5-day lag wind forcing and 3-day lag strong negative SST feedback. Lagged linear regressions are performed onto a reference SST index of the cold tongue northern front in the Gulf of Guinea. A cold SST anomaly covering the equatorial and coastal upwelling is forced after about one week by stronger-than-usual south-easterlies linked to the St Helena anticyclone, suggesting that intraseasonal variability in the Gulf of Guinea is connected to large-scale fluctuations in the South Atlantic. Within about 5°S and 5°N, two retroactions between SST and surface wind appear to dominate near-surface atmosphere conditions. When the wind leads the SST, stronger monsoonal winds north of 2°N are partly sustained by the developing SST anomaly and bring more humidity and rainfall toward the continent. When the SST leads the wind, a reversal of anomalous winds is observed mainly south of 2°N, closing a negative feedback loop with a biweekly periodicity. Eventually, further investigation with an ocean model emphasizes the contribution of the horizontal advection in shaping these intraseasonal SST signals. The contribution of vertical processes may also be important but was more difficult to estimate. Copyright © 2010 Royal Meteorological Society

KEY WORDS air–sea interactions; statistical analysis

Received 14 December 2008; Revised 7 October 2009; Accepted 9 November 2009

1. Introduction

The eastern equatorial Atlantic (EEA) exhibits a pronounced annual cycle in sea-surface temperature (SST), surface wind, and deep convective activity (Mitchell and Wallace, 1992; Li and Philander, 1997; Gu and Adler, 2004). Figure 1 shows the bi-monthly means of SST, spatially smoothed precipitation and surface wind, during March–August for 2000–2007 (see section 2 for the data description). The SST is maximal in boreal spring when the intertropical convergence zone (ITCZ) comes near the Equator; in March–April, it displays a broad meridional gradient (from 27 to 31°C) in the Gulf of Guinea. The ITCZ, depicted by the belt of maximum precipitation, is also quite broad and stands slightly north of the Equator. Precipitation is maximum around 3°N west of 10°W where southerlies meet northerlies. Then, the northward migration of the ITCZ brings stronger winds northward, accelerating the equatorial upwelling (or 'cold tongue'); the SST progressively cools from April to July with a minimum in the latitudinal band between 4°S and 1°N and near the southern coast of Africa. While the marine ITCZ west of 10°W coincides with the convergence of surface winds around 7°N, to the East the precipitation maximum sticks to the south of the Gulf of Guinea coastlines (around 4°N). By the end of June/early July, this maximum makes a sudden northward jump and joins the central ITCZ latitude around 10°N (Sultan and Janicot, 2003). The Atlantic cold tongue is then well developed with coldest temperatures spanning south of the Equator and off the African coasts, and a large northward SST gradient up to about 4°N.

Li and Philander (1997) suggested that the SST variability in the Gulf of Guinea would be a passive response of the ocean to seasonal winds, the latter being themselves a passive response to seasonal temperature changes in the West African continent. In contrast, it is commonly thought that the interannual variability of the Atlantic equatorial upwelling, and the associated meridional SST gradient over the Gulf of Guinea, play a role in the northward shift of the African monsoon and the intensity of the related rainfall (Lamb, 1978a, 1978b; Opoku-Ankomah and Cordery, 1994; Kouadio *et al.*, 2003; Sultan and Janicot, 2003; Gu and Adler, 2004; Okomura and Xie, 2004) through ocean–atmosphere interactions. The equatorial SST influences the winds through thermodynamic or dynamic feedbacks, local or remote (Klein and Hartmann, 1993; Chang and Philander, 1994; Xie and Philander, 1994). They are thought to happen at short time-scales of less than one month or two, due to the fast dynamical response of equatorial atmosphere and ocean. Regarding

*Correspondence to: G. de Coëtlogon, LATMOS-IPSL, Université Pierre et Marie Curie, 4 place Jussieu, 75252 Paris Cedex 5, France. E-mail: gdc@latmos.ipsl.fr

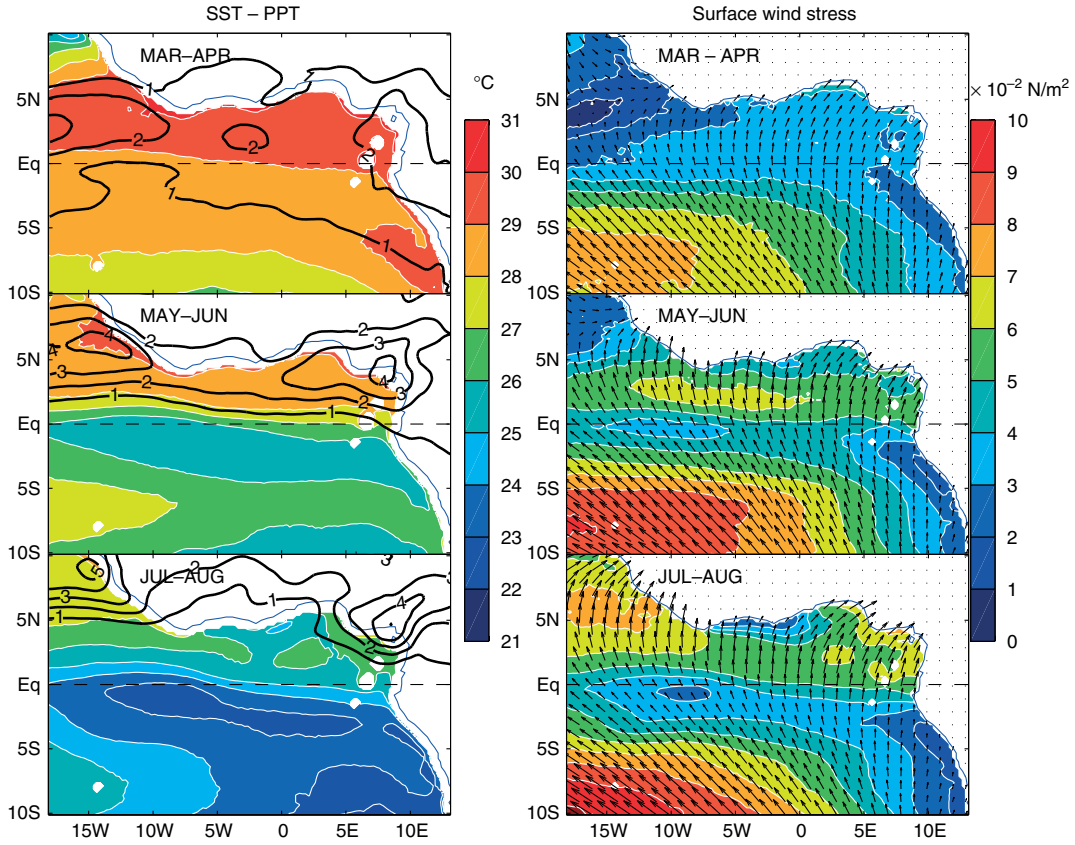

Figure 1. 2000–2007 bimonthly means. Left: TMI SST (colours,°C) and TRMM rainfall (black contours, mm/day). Right: QuikSCAT surface wind-stress (one arrow on 4×4 plotted for clarity) with magnitude (colours, N/m^2). This figure is available in colour online at www.interscience.wiley.com/journal/qj

the influence of warm (above 26–27°C, depending upon region and season, Graham and Barnett, 1987; Waliser *et al.*, 1993) tropical SST on the local atmosphere at short time-scales, the following two mechanisms have been historically proposed. The first is based on the pressure gradient in the near-surface atmosphere induced by the SST gradient; linear dynamics of this mechanism have been described in Lindzen and Nigam (1987), Mitchell and Wallace (1992) or Young (1987). The second mechanism relies on elevated latent heating by deep convection, which is thought to be a major driver of equatorial surface winds (Gill, 1980), where a warm SST anomaly (SSTA) would favour convection and thus convergence of surface winds. Note that the response of the wind to an SSTA is expected to be mathematically similar for both mechanisms and thus hardly differentiable (Neelin, 1989). Back and Bretherton (2009) recently showed that the distribution of convergence in tropical surface zonal winds is largely due to boundary-layer temperature gradients, closely related to SST gradients; the latter would thus be a cause rather than a consequence of the deep convection distribution.

In 'cool' tropical areas (SST below the 26–27°C threshold), air–sea interactions are poorly understood (Xie, 2004). The atmospheric response to SST fluctuations is likely to be trapped within the planetary boundary layer (between 1000 and 2000 m deep) because this layer is capped by a stable layer, often in the form of a temperature inversion (Norris, 1998). Sweet *et al.* (1981), Wallace *et al.* (1989) and Hayes *et al.* (1989) suggested that the positive SST–wind-speed correlation generally observed in tropical regions is due to a modification of the marine atmospheric boundary layer (MABL) stability induced by small-scale features in the SST field, leading to a vertical shear adjustment. Cooling over cool water increases stratification and stabilizes the MABL, inhibiting vertical mixing by turbulence and convection. This decouples the surface winds from the stronger winds at heights of 100 m or more, and increases the wind shear near the sea surface. Conversely, heating over warm water decreases stratification and destabilizes the MABL, enhancing vertical turbulent mixing and convection. It deepens the MABL and mixes momentum downward from aloft, decreasing the wind shear near the sea surface. This effect can be distinguished in the seasonal cycle shown in Figure 1, where minima in the wind-stress magnitude and the SST strikingly coincide, especially in May–August. It has been studied in the eastern Pacific with high-resolution satellite data by Chelton *et al.* (2001), who showed the remarkable spatial and temporal coincidence between surface wind-stress perturbations and SST, oscillating with tropical instability waves (TIW) at intraseasonal time-scales. Most of the studies based on vertical soundings of the atmosphere support the validity of this mechanism (Wallace *et al.*, 1989; Hashizume *et al.*, 2002). However, the height

DOI: 10.1002/qj

reached by the vertical shear adjustment is still unclear, and some recent radiosonde observations suggest that the wind adjustment occurs over the whole depth of the MABL, rather than following a log-profile adjustment (Xie, 2004; Samelson *et al.*, 2005; Small *et al.*, 2005, or see Small *et al.* (2008) for an exhaustive review). Differential heating of the MABL on opposite sides of an SST front also tends to create a pressure gradient force, following the Lindzen and Nigam (1987) mechanism, which could eventually generate secondary circulations (Hsu, 1984; Wai and Stage, 1989).

The goal of the present paper is to provide a statistical basis for the analysis of air/sea linear interactions in the Gulf of Guinea, based on observations with very high temporal and spatial resolution, thanks to satellite products which are now available for periods long enough to establish climatologies of intraseasonal variability. A focus is made on the spring and summer months, when the ITCZ migrates from its southernmost (around the Equator) to its northernmost latitude (around 10°N), because particularly strong air–sea interactions are then suspected to be responsible for the cold tongue settlement and the ITCZ's fast northward migration.

2. Data

2.1. SST and surface winds

QuikSCAT (Quick Scatterometer) winds and TMI (Tropical Rainfall Measuring Mission (TRMM) Microwave Imager) SST data were retrieved from Remote Sensing Systems website (www.remss.com), sponsored respectively by the National Aeronautical and Space Administration (NASA) Earth Science REASoN DISCOVER Project and Ocean Vector Winds Science Team. Four main datasets covering two different regions with different resolutions were constructed from the original datasets. The first covers the Gulf of Guinea (18°W–13°E/10°S–10°N) on the original 1/4° grid. The second covers the South Atlantic (80°W–20°E/37°S–37°N) and is interpolated on a 1° grid. Only data from 2000 to 2007 were extracted, covering a period of eight years. Retrieved data were daily, but filtered with a 3-day running mean due to the lack of daily overlapping satellite tracks. Remaining missing points (presence of rain) were filled using a cubic spatial interpolation and a few missing days were completed with temporal linear interpolation at each grid point. Total column water vapour (thereafter TCWV) was also retrieved from the TMI data and treated similarly.

The surface wind stress was computed from the surface winds direction and velocity, using the bulk aerodynamic formula $\tau = \rho C_{\mathrm{d}} v_{10} v_{10}$, where ρ is the air density (taken here to be 1.025 kg/m^3) and C_{d} is the drag coefficient for neutrally stable conditions. The latter was computed using the modified Large and Pond (1981) drag coefficient described in the appendix of Large *et al.* (1994), which is the formulation most commonly used for scatterometer applications.

2.2. ECMWF data

Sea-level pressure (SLP), geopotential height at different pressure levels, surface solar radiation (SSR), surface latent heat flux (SLHF) and TCWV with a resolution of 1.125° from the European Centre for Medium-Range Weather Forecasts (ECMWF) ERA40 reanalysis were retrieved thanks to the ClimServ data server (climserv.ipsl.polytechnique.fr), and the four-daily data were daily averaged. As the ERA40 data are available only until mid-2002, the same fields were retrieved from the ECMWF meteorological products from the operational analysis over the period mid-2002 to 2007. This use of two different kinds of data (reanalysis before 2000 and operational analysis afterwards) is of course problematic; moreover, the different model versions used by ECMWF for the operational analyses could have introduced some artificial discontinuities in the time series. However, results were less interesting when using other products, complete over 2000–2007 but with a poorer spatial resolution.

2.3. TRMM rainfall product

Daily mean precipitation in 2000–2007 from the TRMM 3B42 product incorporates several satellite measurements including the TMI and TRMM Precipitation Radar to calibrate infrared precipitation estimates from geostationary satellites (Huffman *et al.*, 2001). They were retrieved from their website (trmm.gsfc.nasa.gov).

2.4. Oceanic data

A MERCATOR simulation on its most recent configuration, Orca025_lim-T09, was chosen because of its high horizontal (0.25°) resolution and its 3-day output frequency. It was forced using the ECMWF surface data (surface air temperature and relative humidity, total cloudiness and precipitation, 10 m wind speed, and wind-stress) with no data assimilation (see Garric *et al.* (2008) for further specifications of the simulation). The turbulent fluxes, ongoing and outgoing radiation and albedos (over sea and sea ice) were calculated using an empirical bulk parametrization. Temperature and horizontal currents at all levels were available from 2000 until May 2007.

3. Statistics of the air–sea interaction in the Gulf of Guinea

In order to focus on daily and weekly time-scales, SST and surface wind-stress data were filtered using a Lanczos high-pass filter with a 90-day cut-off, thereby removing seasonal and longer time-scales (note that the use of a shorter cut-off of 60 days does not change the results significantly). Days from 1 March to 31 August were then selected (2000–2007) and an empirical orthogonal function (EOF) decomposition performed on both fields. The first mode of SST variability catches more than 14% of the total variance, and the first mode of surface wind-stress almost 20% (Figure 2). Second modes are well

DOI: 10.1002/qj

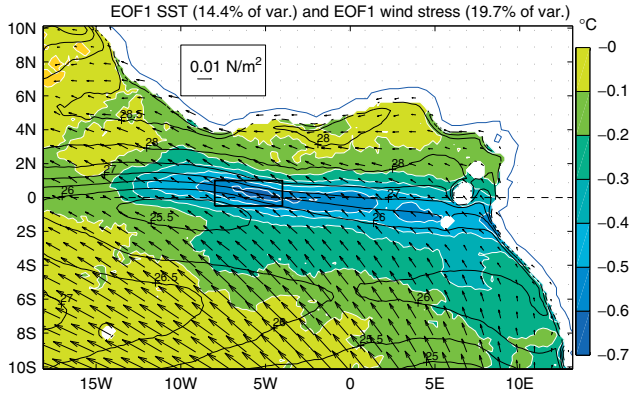

Figure 2. EOF 1 of high-pass filtered TMI SST (°C, colours) and QuikSCAT surface wind-stress (arrows). Black contours: mean SST TMI for MAMJJA 2000–2007 (°C, interval contours of 0.5°C). Black frame: reference area for the Northern Cold Tongue Index (NCTI). This figure is available in colour online at www.interscience.wiley.com/journal/qj

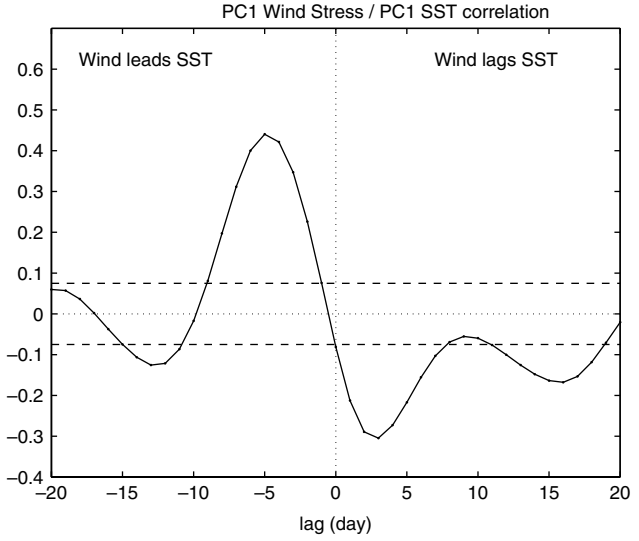

Figure 3. Lagged cross-correlation between the first modes of SST and surface wind-stress (plain line) with 10% significant correlation (dashed lines). The atmosphere leads the ocean at negative lags.

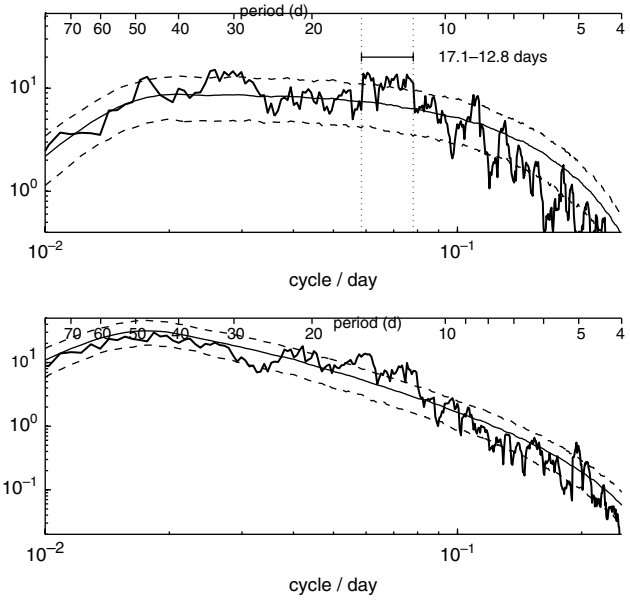

Figure 4. Top: four-window multi-taper power spectrum of the first principal component of the surface wind-stress in the Gulf of Guinea (heavy), with the mean spectrum of simulated AR1 of the same variance and persistence (thin). Dashed lines: 10 and 90% significance levels. Bottom: same as top for the first principal component of the SST.

separated from the first modes since they both catch less than 6% of the total variance (not shown). In the first mode, the SST anomaly is maximal on the northern front of the mean cold tongue (Figure 2, in colour), following roughly the Equator where the mean meridional SST gradient is maximal (see black contour). The leading mode of the wind-stress corresponds to fluctuations of southeasterlies south of the Equator, which turn into easterlies further north (Figure 2, arrows).

The lagged cross-correlation of both principal components (PC1) suggests the existence of a very strong link between the two modes (Figure 3). For comparison, the 10% significant level for zero correlation is computed with an estimated persistence of 3 days for the wind-stress PC1 from its autocorrelation (Von Storch and Zwiers, 1999), giving 0.075. A very high correlation (more than 0.4) is found at lag −5, implying that anomalously strong (weak) southeasterlies lead a negative (positive) SST anomaly with a maximum when the wind stress leads the SST by 5 days. A strong negative correlation is also found around lag 3, meaning that colder-than-normal (warmer) SST conditions in the northern front of the cold tongue lead a weakening (strengthening) of the southeasterlies by a few days (minimum at lag 3). This could correspond to a negative feedback between SST and wind-stress fluctuations at short time-scales.

However, this statistical relationship between the two fields does not prove that the SST influences the overlying wind stress at this spatial scale. Indeed, a periodicity of about 15 days is clearly visible in the lagged correlation, as the negative correlation is found again around lags −13 and 16 (Figure 3). The corresponding peak in the 11–17-day band in the power spectrum of the surface wind-stress PC1 (Figure 4, top) is highly significant, since it lies above the 90% level after having been tested against the spectrum of one thousand AR-1 time series with the same variance and short persistence (and beforehand similarly filtered with a 3-day running mean and 90-day high-pass filtering). The fortnight peak in the winds of the Gulf of Guinea was found in previous studies (Garzoli, 1987; Houghton and Colin, 1987; Grodsky and Carton, 2001; Mounier *et al.*, 2008) and could alone explain a large part of the biweekly variability observed in the wind/SST lagged cross-correlation in Figure 3. On the other hand, it was also found in the spectrum of the SST principal component (Figure 4, bottom). Such a peak in the SST is clearly linked to Tropical Instability Waves (TIW) in the equatorial eastern Pacific or central Atlantic, where they are free to evolve, tightly coupled with overlying wind fluctuations, and contribute a lot to energy propagation (Chelton *et al.*, 2001; Jochum *et al.*, 2007). But east of 10°W

DOI: 10.1002/qj

in the tropical Atlantic, the sea-surface height anomaly and thermocline variations at 10–40-day periods result mostly from Rossby-gravity (or Yanai) waves excited by the quasi-biweekly meridional winds (Garzoli, 1987; Houghton and Colin, 1987; Bunge *et al.*, 2006; Athié and Marin, 2008; Guiavarc'h *et al.*, 2008; Han *et al.*, 2008). Therefore, in the EEA, the biweekly variability could initially be a characteristic of the atmospheric circulation alone, which would transmit it to the passive responding SST, with a possible amplification from wind-forced Yanai waves since its responding frequency coincides with the fortnight peak. In this case, the biweekly variability would also be found in the atmospheric circulation at larger spatial scales; the next section examines this hypothesis and shows its unlikelihood.

The alternative hypothesis of a negative feedback resulting from a local oceanic influence on surface winds is addressed in section 5, but its impact can already be measured as follows: the biweekly variability is expected to raise a significant minimum in the autocorrelation of the SST PC1 at lag 7, which amounts to roughly -0.2 (not shown). In the cross-correlation between the SST and wind-stress PC1 (Figure 3), 0.4 is found when the wind leads by 5 days, and -0.3 when it lags by 3 days; therefore, the negative SST/wind feedback would explain $-0.4 \times 0.3/-0.2 = 60\%$ of the SST PC1 autocorrelation at lag 7, i.e. 36% of the biweekly wind variance in the Gulf of Guinea.

4. Large-scale atmospheric signal linked to the eastern equatorial SST

An index of SST intraseasonal oscillations on the northern front of the cold tongue (hereafter NCTI, 'northern cold tongue index') was built by averaging the high-pass filtered SST in the 8°W–4°W/0.5°S–1°N area (see framed area in Figure 2). This region was chosen since the SST variance at intraseasonal time-scales is maximal there, as seen in the first EOF pattern (Figure 2) or in the root mean square (r.m.s.) map of intraseasonal March–August (MAMJJA) SST (not shown). The different anomalies projected onto the NCTI were computed by removing the MAMJJA mean from the original field. Simple linear regressions were performed by computing at each grid point the correlation between the anomalous field and the NCTI, weighted by the r.m.s. of the field *with a minus sign*; therefore, they show the anomalous pattern linearly correlated with a one standard-deviation *negative* anomaly of the NCTI (about -1°C). Lagged regressions (i.e. between the field and the NCTI lagged in days, Figures 5, 6 and 10) provide a useful insight on the linear relationship between the most variant eastern equatorial SST and atmospheric circulation, since it allows for a preliminary sorting of causes and consequences inside the ocean–atmosphere coupling phenomenon.

The lagged regression of the surface wind-stress on the NCTI in the South Atlantic is plotted in Figure 5, as well as the regression of ECMWF SLP and SST. For example, lag -6 shows the surface wind-stress anomaly significantly correlated with a cold SST anomaly occurring 6 days later in the EEA, together with the corresponding patterns of SLP and SST. By definition, the SST anomaly reaches a minimum of about -1°C at lag 0, i.e. 5 or 6 days after the southerlies maximum, in agreement with the delay shown in the lagged cross-correlation in Figure 3. A remarkable feature is that the stronger-than-normal southeasterlies in the Gulf of Guinea clearly belong to a wide basin-scale pattern, mainly an anomalously strong anticyclonic circulation over the South Atlantic basin. This wind-stress anomaly is in very good agreement with the SLP anomaly, which also shows a stronger-than-normal St Helena anticyclone centred around 10°W/30°S at lag -4 (note that a slight eastward displacement of the anticyclonic cell is observed from lags -6 to -2). It is clearly barotropic since it can be found in the geopotential height anomaly as high as 100 hPa (not shown). Moreover, the NCTI and the pattern of wind-stress anomaly at lag -5 are correlated by more than 0.3 (not shown), which suggests than almost 10% of the NCTI variability would be controlled by intraseasonal fluctuations of the St Helena anticyclone.

From lag -1 to 1, the large-scale anticyclone vanishes and a divergent wind-stress pattern appears above the cold SSTA, together with a positive SLP local anomaly. This could correspond to a response of surface winds to the development of the cold SST through the SST-gradient induced mechanism (Lindzen and Nigam, 1987), or a latent heating response in spring when equatorial SST is still favourable to deep convection (Gill, 1980), but a closer look shows that the largest northward wind-stress anomalies are not exactly superimposed on the strongest anomalous SST gradient (see section 5). Moreover, the SLP anomaly actually follows the wind divergence rather than precedes it. Since the reversed anomalies are the largest at lag 2, i.e. 8 days after the strongest cyclonic anomalies at lag -6, it fits the biweekly spectral peak found previously. Hence, we suggest this divergence is mostly SST-induced: right at the Equator, the cold SSTA reverses progressively the initial wind-stress anomaly, constituting the negative feedback discussed at the regional scale in section 3 and studied in more detail in section 5.

The progressive reversal of anomalous southeasterlies takes place over the whole Gulf of Guinea (Figure 5, lags 1–5). Reversed wind anomalies could also be a part of the large-scale atmospheric circulation, since the wind anomaly in the Gulf of Guinea at lag 4 turns around a cyclonic cell centred around 5°W/25°S in the eastern half of the South Atlantic. Altogether, two other concomitant anomalous cyclonic circulations can be observed, one in the western half of the basin and the other above the Angola–Benguela coastal upwelling near 15°S. These three cells are visible in the regression of surface winds as well as in the SLP regression. Interestingly, the SLP anomaly of the latter (lag 3 to 5) develops right above the maximum coastal upwelling SST anomaly, with a few days lag comparable to the chronology of the Gulf

DOI: 10.1002/qj

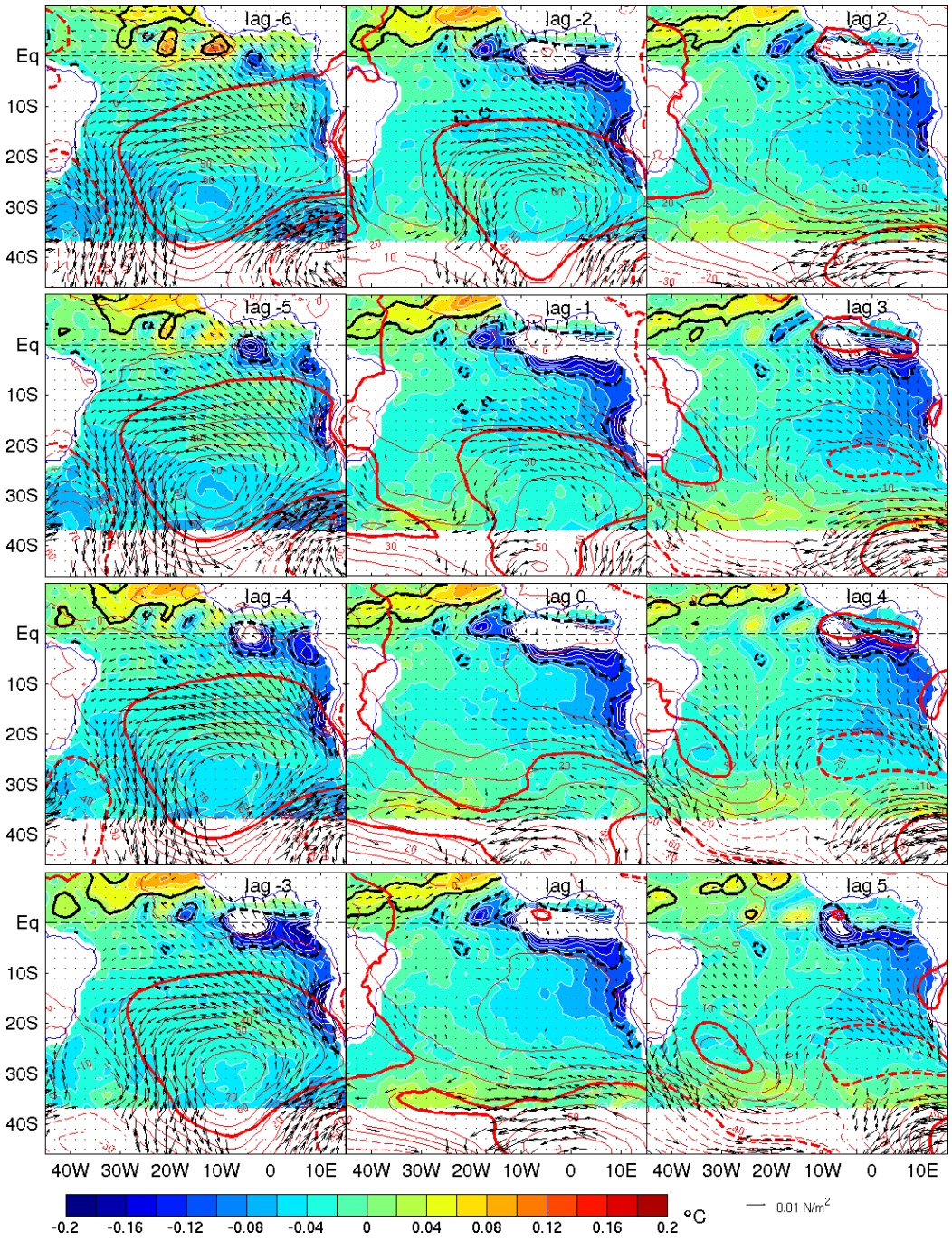

Figure 5. Lagged regressions of three different anomalous fields onto the NCTI. Arrows: QuikSCAT surface wind-stress (one arrow on four when 10% significant). Red contours: ECMWF SLP (Pa, interval contours of 10 Pa). Colours: TMI SST (°C, interval contours of 0.02°C). Heavy black lines (plain for positive, dashed for negative) indicate the 10% level for point correlation between the SST and the NCTI. Heavy red lines: *idem* for the SLP. For clarity, SST anomaly colder than −0.2°C was left blank. The NCTI lags (i.e. the atmosphere leads the ocean) at negative lags. Lags in days, from top to bottom and left to right. This figure is available in colour online at www.interscience.wiley.com/journal/qj

upwelling. This result suggests the existence of a local retroaction, albeit weaker than at the Equator, of the SST on the atmospheric circulation over the Angola upwelling, in agreement with recent studies of eastern boundary upwelling systems (Sow and Marchesiello, personal communication).

Regarding the mechanisms of the biweekly variability in the Gulf of Guinea, one could interpret the above results as deriving solely from the large-scale fluctuations of the circulation in the whole South Atlantic, with a stronger-than-normal St Helena anticyclone giving way to reverse winds after about one week. However, several features contradict this hypothesis. First, surface wind anomalies at lags −4 and 3 in the Gulf of Guinea are not exactly linearly opposite, since the cyclonic anomaly at lag 3 is shifted 5° northeastward with regard to the anticyclone at lag −4. In addition, the east equatorial signal seems to be dissociated from the anticyclone at lags 0 and 1, before reconnecting to it from lag 2 onwards. Moreover, while the first EOF of surface

DOI: 10.1002/qj

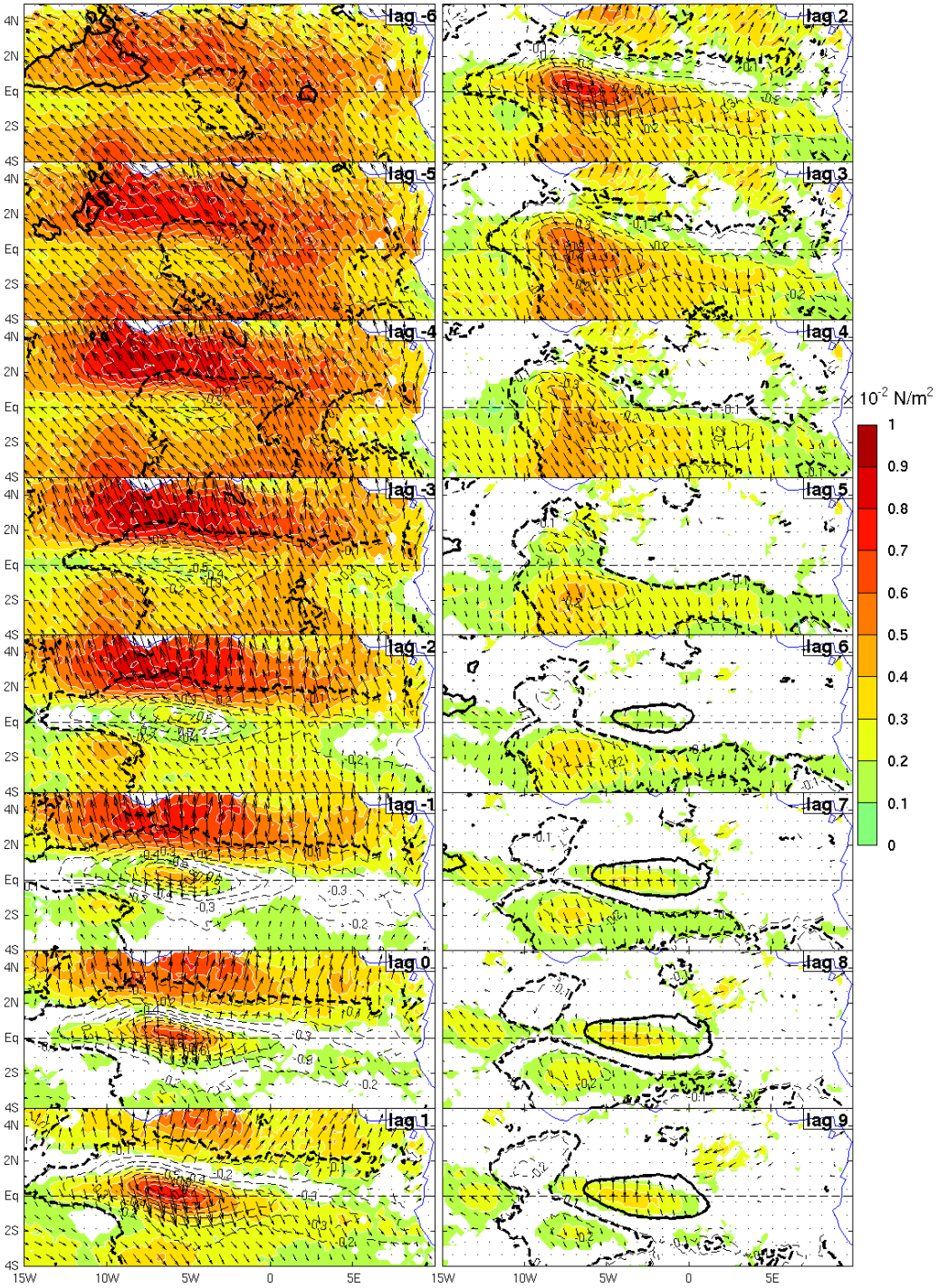

Figure 6. Same as Figure 5, but zoomed into the Gulf of Guinea, from lag −6 (top left) to 9 (bottom right). Colours stand for the anomalous magnitude of the surface wind-stress (interval contours of 0.1×10^{-2} N/m^2) when significant. Black contours: ECMWF SST (interval contours of 0.1°C). Heavy black (plain for positive, dashed for negative): 10% significant correlation between the SST and the NCTI. This figure is available in colour online at www.interscience.wiley.com/journal/qj

winds on the whole South Atlantic basin corresponds well to a more or less intense St Helena anticyclone, it does not exhibit a significant biweekly variability (not shown). Thus, although a substantial part (more than 10%, as seen previously) of the variability in the Gulf of Guinea is controlled by the large-scale circulation in the South Atlantic, we claim that a large part of the biweekly variability rather stems from the regional negative feedback between SST and surface winds. Eventually, it could also be in part a response of the whole Hadley cell to the cold SSTA in the EEA, since the positive SLP anomaly over the cold tongue develops slightly in advance of the negative SLP anomaly around 0°–10°E/20°–30°S. The study of the deep atmospheric response to the tropical SST forcing is beyond the scope of the present paper, but this is obviously an interesting hypothesis which will need further investigations.

DOI: 10.1002/qj

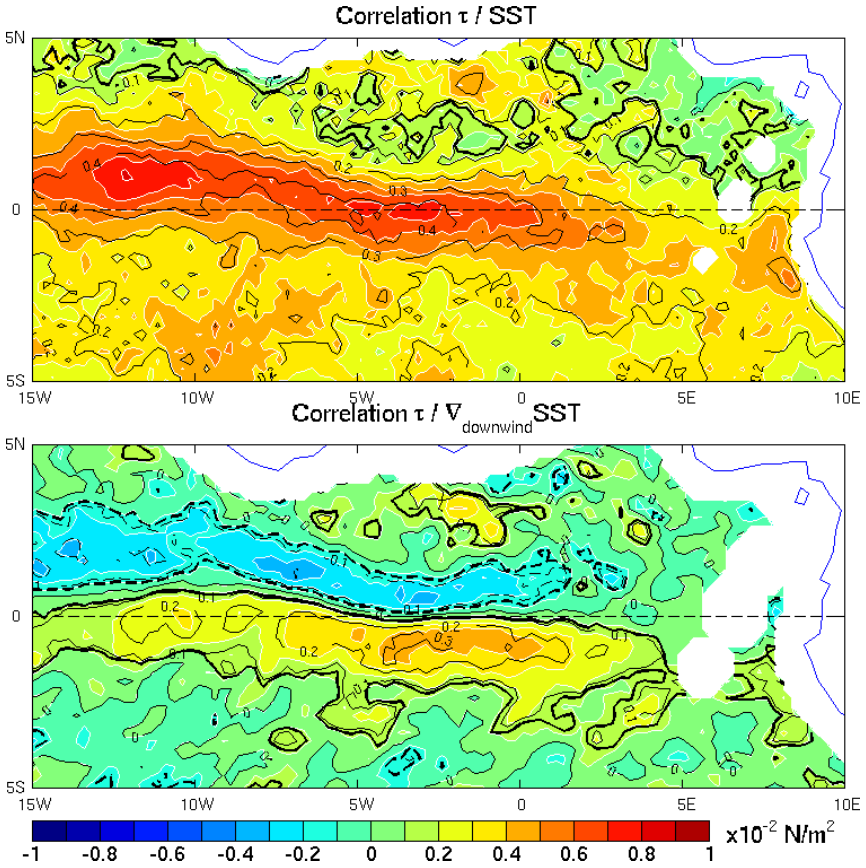

Figure 7. Point correlation between the high-pass filtered magnitude of the wind-stress and the SST (top) or the downwind gradient of SST (bottom), when the wind lags the ocean by 2 days (black contours, interval of 0.1). Correlations are multiplied by the r.m.s. of the wind-stress anomaly, in order to show the response of the wind in N/m^2 to a fluctuation of SST or SST gradient of one standard-deviation (colours). Heavy black contours show the 10% significant correlation. This figure is available in colour online at www.interscience.wiley.com/journal/qj

5. Regional air–sea feedbacks

Intraseasonal interaction between SST and surface winds are now examined specifically in the vicinity of the most variant SST at intraseasonal time-scales in the Gulf of Guinea, still accounted for by the NCTI defined in the last section: the simple linear regressions shown in Figure 5 were zoomed between 4°S and 5°N (Figure 6). By definition, the SSTA is the coldest (about −1°C) at lag 0, i.e. 5 or 6 days after the anomalous wind-stress is maximal over most of the Gulf of Guinea. Therefore, the persistence of the cold SSTA and the time it takes to decrease or increase is slightly less than one week. In parallel, south of 2°N, a progressive deceleration of the north-westward wind-stress anomaly is observed when passing over the growing cold SSTA, as well as a slight westward deviation of its direction from lag −5 to −2. It is southward and maximal at lag 2. North of the SST anomaly front (between 1 to 2°N), on the contrary, the northward wind-stress anomaly increases between lags −6 and −3 and persists until lag 2. These clear opposite tendencies result in a wind divergence settling at lag −1 on the northern side of the cold SSTA. The wind-stress anomaly coincides spatially very well with the SSTA, albeit with a small lag of one or two days: the lowest SSTA at lag 0 stands right on the maximum of the southward wind-stress anomaly (up to 0.9 N/m^2 at lag 2). From lag 3 onwards, this cold SSTA splits in two lobes on either side of the Equator, with an overlaid southeastward wind-stress anomaly. Meanwhile, a warm SSTA settles between 3°W and 0° at lag 6 and increases until lag 9, coming with a northward anomaly of surface wind-stress perfectly matching the SST pattern.

The striking similarity between anomalous SST and wind-stress magnitude in Figure 6 strongly emphasizes the SST influence on surface winds originally described by Sweet *et al.* (1981), Wallace *et al.* (1989) and Hayes *et al.* (1989) in the Pacific. As the mean surface wind-stress is mainly northwestward in this region (Figure 1), a cold (warm) SSTA decelerating (accelerating) the wind would create a southeastward (northwestward) wind anomaly. From a more general point of view, a positive correlation of the near-surface wind speed and SST is indeed generally observed near equatorial SST fronts and is considered as traducing the influence of SST on overlying winds through the perturbation of vertical stability in the MABL (Liu *et al.*, 2000; Chelton *et al.*, 2001; Hashizume *et al.*, 2002; Xie, 2004; Small *et al.*, 2008). The map in Figure 7 (top) qualifies and quantifies this SST feedback through correlations (in black contour) between the MAMJJA high-pass filtered SST and 2-day lagged wind-stress anomalies in the Gulf of Guinea; it is significant over most of the region, and positive with a maximum along the Equator east of 5°W or along 1°N

DOI: 10.1002/qj

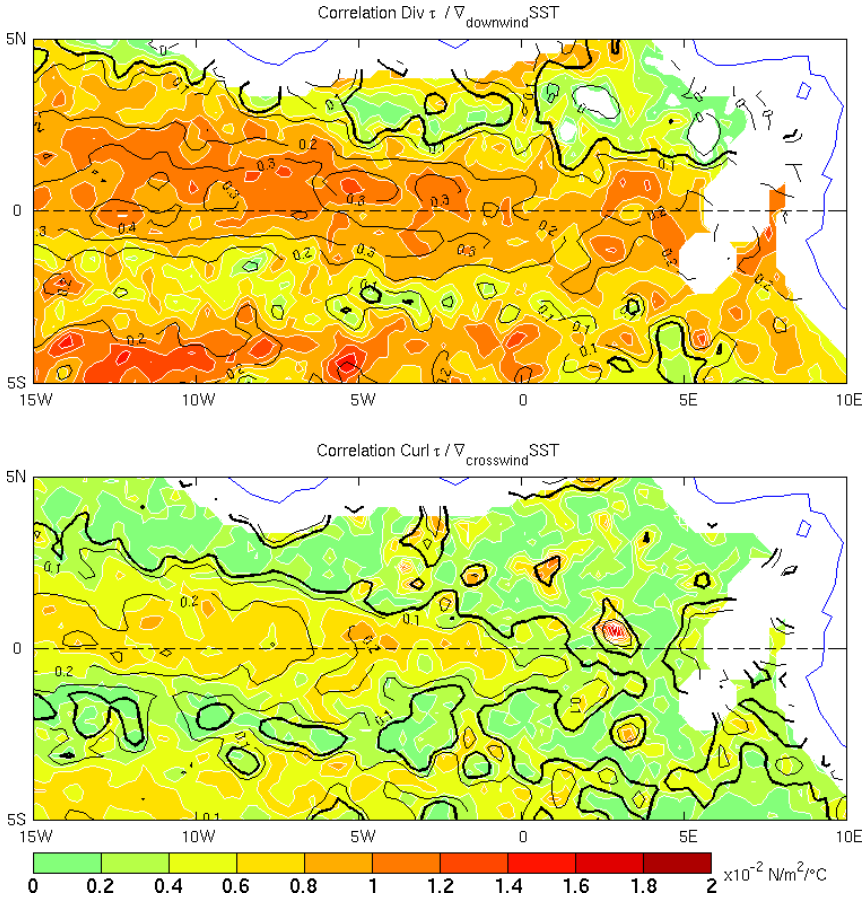

Figure 8. Top: point correlation between the high-pass filtered divergence of the wind stress and downwind gradient of SST (black contours, interval of 0.1) and coefficient of the linear regression (i.e. point correlation times the r.m.s. of the wind-stress divergence anomaly divided by the r.m.s. of the downwind SST gradient anomaly, in colour). Heavy black contours show the 10% significant correlation. Bottom: same thing between the curl of the surface wind-stress and the crosswind gradient of SST. This figure is available in colour online at www.interscience.wiley.com/journal/qj

further west, coinciding with the largest anomaly in the EOF1 of SST (shown in Figure 2, see also the cold SST anomaly at lag 0 in Figure 6), plus a strong westward extension. (Note that at negative lags, i.e. smaller than -1 or -2 days, the correlation is generally negative, traducing the well-known forcing of the cold tongue by surface winds, not shown.) Correlation spans from $+0.2$ to $+0.3$ in the southern part of the domain to $+0.4$ to $+0.5$ around the Equator, meaning that the SST can explain respectively more than 5–10% and up to 25% of the wind-stress variances there. A local SST fluctuation of one standard-deviation corresponds to a wind-stress change of $3–4 \times 10^{-3}$ N/m^2 in the south and 7×10^{-3} N/m^2 near the Equator. The importance of the phenomenon at the Equator is highlighted when compared with the seasonal mean stress there (about 4×10^{-2} N/m^2, Figure 1). Again, these values are found maximal when the ocean leads the wind by 1 or 2 days, likely corresponding to the time necessary for the atmospheric column to adjust to the SST anomaly, but it is already significant at lag 0 over a wide band straddling the Equator (not shown).

The SST-induced changes of atmospheric stability and its consequent overlying wind-stress anomaly can be better characterized with the wind direction relative to the SST gradient. Following Chelton *et al.* (2001, 2004), the wind-stress response to geographical variations of the underlying SST field was quantified by performing simple linear regressions between the divergence of the wind stress and the downwind gradient of SST (Figure 8, top) and between the curl of the wind-stress and the crosswind gradient of SST (Figure 8, bottom) at each grid point (see for example O'Neill *et al.* (2003) for details on computing the downwind and crosswind SST gradients; a spatial smoothing on 3×3 square grids compensates error amplification due to the computing of the curl and the divergence of the wind stress.) Correlations are plotted in black contours. Both maps show generally significant correlations, with largest values following the Equator/1°N line (up to 0.2 for the curl/crosswind, and 0.3–0.4 for the divergence/downwind; the difference between the two responses may be due to the finite time-scale of boundary-layer adjustment (Chelton *et al.*, 2001)). The regression coefficients around the Equator are in good agreement with the ones previously found for the strongest SST fronts in the world, namely about 1×10^{-2} N/m^2/°C (respectively 0.6×10^{-2} N/m^2/°C) for the divergence/downwind (resp. curl/crosswind) regression in the Kuroshio and Gulf Stream regions. It is however slightly weaker than in the Tropical Pacific

DOI: 10.1002/qj

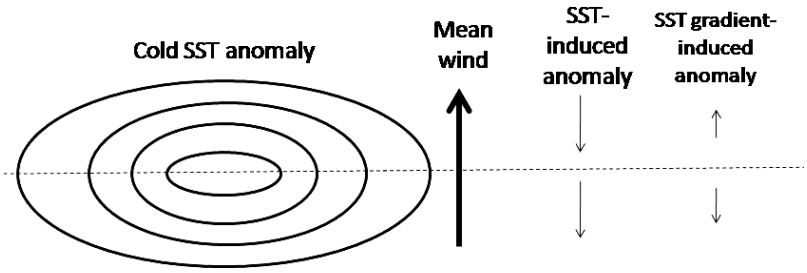

Figure 9. The two possible responses of the surface wind to an idealized cold SST anomaly/mean surface wind pattern.

where 1.9×10^{-2} N/m^2/°C (resp. 0.8×10^{-2} N/m^2/°C) was found (Chelton *et al.*, 2004, their figure 4). Still, they clearly show that the SST imprints very significantly the atmosphere at intraseasonal time-scales during boreal spring and summer in most of the EEA.

The second main possible mechanism relevant for our results is the control of surface winds by the SST-gradient-induced pressure gradients (Lindzen and Nigam, 1987). Figure 7 (bottom) shows an attempt to quantify this effect by correlating the downwind (roughly meridional) SST gradient with the wind-stress magnitude at each grid point, when the wind lags the SST by 2 days. Positive correlations suggest acceleration (deceleration) of the wind when forced by a positive (negative) SST gradient, according to this mechanism. However, the significant values are relatively modest and surprisingly confined to the immediate south of the Equator. Moreover, negative values north of the Equator suggest the opposite mechanism. This supports an overall lesser control of the SST gradient over the winds relative to the SST-induced mechanism; it can be easily understood in the light of a cold SST anomaly – keeping in mind that it is the dominant pattern of variability – underlying a mean southerly wind, as sketched in Figure 9: while the SST-induced anomalous wind is southward on both sides of the Equator, the anomalous winds induced by the gradient are opposite (northward in the north, southward in the south). Hence, in Figure 6 (lag 2), the wind response is rather weak around 1–2°N where the two effects are opposite, whereas it is strong over the whole seasonal cold tongue along and south of the Equator, where the two effects are in the same direction. Overall, the SST-induced effect on the wind clearly dominates, with strongest southward (northward) wind-stress anomalies coinciding with coldest (warmest) SSTA. It results in the regional negative feedback observed at the biweekly frequency in the Gulf of Guinea.

However, due to thermal advection, the length scale over which the atmospheric temperature adjusts over the whole MABL may be longer than the SST frontal width; the air temperature and resulting hydrostatic pressure gradients could hence be located downstream of the SST gradient (Chelton *et al.*, 2001; Small *et al.*, 2008), i.e. further north. This effect cannot be accounted for by the local correlation previously discussed, but could explain a part of the anomalous strong southerlies observed north of about 2°N from lags −6 to 1 in Figure 6. Initially belonging to the large-scale wind pattern (Figure 5), the latter are maximal at lags −4 or −3 and persist until lag 3 or 4, while turning 90° clockwise (northwestward at first, they are mostly northward around lag 0, and then northeastward). Because of this orthogonal rotation, they cannot be a statistical artefact coming from the biweekly variability of the southeasterly wind-stress forcing and must be strongly forced by the cold SSTA in development. However, while clearly involved, the oceanic influence cannot explain why the maximum of these southerlies occur at lag −2, i.e. 2 days before the SST or SST gradient anomalies are maximal. This could rather be due to the interaction between the ocean and the continent, although the linear regression of SLP onto the NCTI does not lead to any significant signal over the continent (maybe due to the flaws in the data discussed in section 2.2). Another possibility is that these strong southerlies would be linked with the continental front (a strong convergence induced by the meeting of the marine winds with the continent), or with a larger-scale signal. However, the only robust SLP signal is the anomalous high anomaly observed above the cold anomaly in the centre of the anomalous wind-stress divergence from lags 1 to 5 (Figure 6): northward at first, when the SLP gradient between the ocean and the continent is still weak, the winds turn progressively eastward, led by the Coriolis deviation around this increasing SLP anomaly. But in short, on the northern front of the SST gradient, increased monsoonal winds are directed toward the continent from lags −5 to 4.

As can be easily foreseen, these southerlies increase the transport of humidity, i.e. precipitable water, over the West African continent. The regression of the TRMM precipitation on the NCTI when the latter lags by 2 days, i.e. when the northward monsoonal winds are the strongest, exhibits increased rainfall widely spread along the West African coast (Figure 10). The TCWV is also projected on the NCTI (Figure 10, black contours) and fits very well with the precipitation anomalies; increase in the latter comes naturally with an increase of the TCWV, which is mostly contained in the atmospheric boundary layer. The maximum of the signal is located over the ocean, but very close to the coast, and a significant part of it spans the coastal regions: this positive precipitation/humidity anomaly could decrease the surface temperature and contribute to lowering the local pressure, sustaining the monsoonal winds (which progressively turn east before being damped) and completing a

DOI: 10.1002/qj

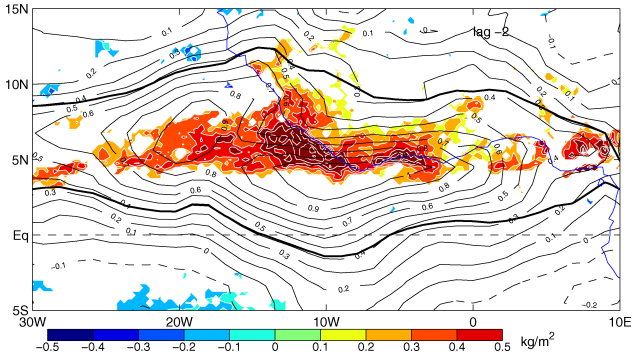

Figure 10. Same as Figure 5 for the TRMM rainfall (colours, mm/day) and total column water vapour (TCWV, black contours, interval contours of 0.1 kg/m^2) anomalies when the NCTI lags by 2 days. Heavy black contour indicates the 10% significant point correlation for TCWV. This figure is available in colour online at www.interscience.wiley.com/journal/qj

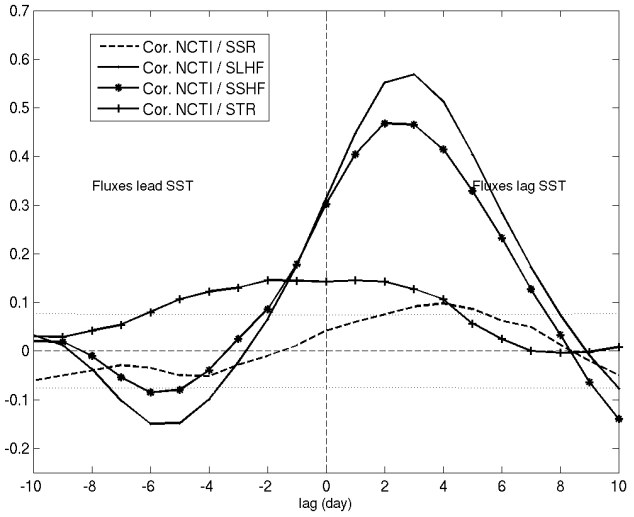

Figure 11. Lagged cross-correlation of the local ECMWF surface heat fluxes with the NCTI. The NCTI leads at negative lags. 10% significant correlation plotted in dotted lines. SSR: surface solar radiation, SLHF: surface latent heat flux, SSHF: surface sensible heat flux, and STR: surface thermal radiation. Fluxes are positive upward.

transient positive feedback loop between the cold SST anomaly and the continent (similar to the one described in Grodsky and Carton (2001) in the West African coastal region further north). Further investigations are needed to explore the dynamics of this atmospheric response to the SSTA. In particular, the importance of the vertical mixing processes in the MABL should be investigated as Hashizume *et al.*(2002) did in the eastern Pacific for TIW-induced perturbations of the surface wind. The question of the continental influence, which is known to be very important in the tropical Atlantic seasonal variability (Xie, 2004) must also be addressed. New appropriate data, such as vertical soundings from the EGEE cruises in 2005 and 2006, or numerical ECMWF reanalysis (ERA interim), would help to address this issue.

6. Origin of SST anomalies

The SSTA is created through thermodynamical air–sea fluxes, horizontal oceanic advection and diffusion, and vertical processes of heat exchange at the base of the oceanic mixed layer. Following for example Chang (1993), neglecting second-order terms and with the assumption of vertically uniform mixed-layer temperature of depth h, the mixed-layer temperature equation can be written as follows, where the anomalies are obtained by removing the MAMJJA mean from the original fields:

$$\frac{\partial T'}{\partial t} = Q_{\mathrm{h}}{}' - Q_{\mathrm{a}}{}' - Q_{\mathrm{e}}{}' - Q_{\mathrm{d}}{}'. \qquad (1)$$

$Q_{\mathrm{a}}{}'$ is the anomalous horizontal advection (i.e. the advection of SST anomalies by the mean current, plus advection of the mean SST by anomalous currents). $Q_{\mathrm{h}}{}'$ is the anomaly of net surface heat flux, $Q_{\mathrm{e}}{}'$ is the anomalous entrainment and $Q_{\mathrm{d}}{}'$ the term of anomalous vertical and horizontal diffusion. We discuss here which of these terms may be the most important in the forcing of the northern equatorial SSTA (i.e. the NCTI) at intraseasonal timescales, and lead to the characteristic patterns observed in Figure 6.

6.1. Air–sea heat fluxes

Air–sea heat fluxes are known to play an important role in SST fluctuations, in particular the latent heat flux through the cooling effect of stronger-than-normal winds, as well as the very intense solar radiation at these low latitudes (Foltz *et al.*, 2003; Peter *et al.*, 2006; Caniaux *et al.*, 2009). In order to estimate the respective parts of latent and sensible heat fluxes (SLHF and SSHF), and thermal (STR, or long-wave) and solar (SSR, or short-wave) radiation in the intraseasonal forcing of the northern cold tongue variability, the corresponding ECMWF data were averaged over the same area as the NCTI (8°W–4°W/0.5°S–1°N). No significant correlation is found in the lagged cross-correlation between the SSR and the NCTI (Figure 11). A significant negative correlation (about −0.15) between the surface latent heat flux and the NCTI is observed when the latter lags the flux by 5 or 6 days, while a much higher positive correlation is found at lag 2 or 3. This result can be interpreted as follows: the latent heat flux anomaly caused by the wind speed acceleration or deceleration seems to contribute a little (it explains 0.15^2, i.e. between 2 and 3% of the NCTI variability) to the formation of the anomaly at negative lags, but once it is created the anomaly is very strongly damped by a reversed flux, likely through wind speed deceleration or acceleration and humidity anomalies. The sensible heat flux contributes also to damp the SST anomaly, but with a smaller impact since its r.m.s. is less than 4 W/m^2 compared to almost 30 W/m^2 for the latent heat flux (not shown). Eventually, the thermal radiation is found to be positive and significant several lags before and after lag 0, meaning that a warm anomaly radiates energy out of the ocean, but also with a minor impact since its r.m.s. is around 10 W/m^2. Note that these results must be treated with caution, since operational analyses are prone to discontinuities. Moreover, ECMWF

DOI: 10.1002/qj

surface heat fluxes are known to suffer significant flaws, especially the latent heat flux, but the latter seem to be quite reliable in the Gulf of Guinea (Kubota *et al.*, 2003), and the use of other latent heat flux data (the OAFlux database: Yu *et al.*, 2008) does not change the results significantly (not shown).

6.2. Ocean dynamics

The role of oceanic processes in shaping the SST anomaly is investigated thanks to a forced MERCATOR simulation of our period of interest. SST and surface current U were computed by averaging the temperature and currents in surface layers, defined as where the temperature varies less than 0.2°C (note that the use of a 0.5°C criterion did not change the results).The bias between the MAMJJA means in the model and the satellite-observed SST is standard for a global ocean model (about 0.5°C in the EEA, not shown). Simulated and observed variances are also in good correspondence, although the amplitude of SST anomalies is sensibly smaller in the MERCATOR simulation (by about 0.2°C). An index similar to the NCTI was computed by averaging the high-pass filtered MERCATOR SST over the same area (8°W–4°W/0.5°S–1°N). The SST regression onto this index (not shown) exhibits a weaker amplitude (also of about 0.2°C), but otherwise is comparable to the observed SST evolution plotted in Figure 6, with a large cold equatorial SST anomaly going westward before splitting into two lobes on either side of the Equator at lag 3, and a warm anomaly appearing between 3°W and 0° at lag 6 with the same apparent westward propagation. Although both propagation velocity and pattern of SST remind one of a slow westward-propagating Rossby wave, no long Rossby wave mode is found in this region between roughly 10 and 35 days of periodicity (Athié and Marin, 2008). A mixed Rossby-gravity wave, or Yanaï wave, may possibly take place but could not be found in the Topex/Poseidon sea-surface height anomalies (not shown) nor in the MERCATOR surface current anomalies. Note that the model is forced by the ECMWF surface fields, which integrate the TMI SST in their assimilation process (operational analyses as well as reanalyses): the strong coupling between SST and 2-metre temperature (and humidity) inevitably coerces the modelled SST into resembling the observations. However, no direct assimilation of the TMI SST was made in the MERCATOR run; ocean dynamics at the origin of the SST fluctuations were hence investigated.

The different terms in (1) were estimated in the Gulf of Guinea between 2000 and 2007 for the March–August period, except for the lateral and vertical turbulent mixing which was not available and probably forms the main part of the residual. The anomalous horizontal advection was computed with the simple scheme: $u'\frac{\Delta\overline{T}}{\Delta x} + v'\frac{\Delta\overline{T}}{\Delta y} + \overline{u}\frac{\Delta T'}{\Delta x} + \overline{v}\frac{\Delta T'}{\Delta y}$, where $\overline{u}$ and $\overline{v}$ are the mean zonal and meridional surface currents in MAMJJA, u' and v' their anomaly. $\overline{T}$ is the mean SST in MAMJJA, and T' the anomaly. The term related to the surface heat fluxes is computed from the ECMWF data, since they are used to force the ocean surface in the model: $Q_\mathrm{h} = \frac{SLHF+SSHF+NPSSR+STR}{\rho_0 C_p h}$, with $\rho_0 = 1023$ kg/m^3, $C_p = 3985$ J/kg/K and h being the mixed-layer depth. Q_h' was obtained by removing the MAMJJA mean. *NPSSR* stands for the non-penetrative part of the surface solar radiation, estimated as follows: $NPSSR = SSR \times (1 - 0.58 \times \mathrm{e}^{-h/0.35} + 0.42 \times \mathrm{e}^{-h/23})$. Eventually, the entrainment was defined by: $Q_\mathrm{e} = \frac{w_\mathrm{e}}{h}\Gamma(w_\mathrm{e})(T - T_\mathrm{r})$, where $w_\mathrm{e} = \frac{\partial h}{\partial t} + h\nabla_h.U$ and Γ is the gate function (i.e. $\Gamma(w_\mathrm{e}) = 1$ if $w_\mathrm{e} > 0$, and $\Gamma(w_\mathrm{e}) = 0$ else), with T_r being the temperature just below the mixed layer. Q_e' was also computed by removing the MAMJJA mean.

The residual was given by $\frac{\partial T'}{\partial t} - Q_\mathrm{h}' + Q_\mathrm{a}' + Q_\mathrm{e}'$. Off-line computing of the entrainment in an ocean general circulation model (OGCM) suffers from large errors, because the temporal resolution of the output (3 days here) does not allow for a sufficiently accurate off-line computation of the term which varies at very high frequencies, especially here in the EEA where the SST gradient is very large and the equatorial thermocline very sharp. The MAMJJA mean fields of (1) are globally in agreement with previous studies (Peter *et al.*, 2006) and emphasize the net surface heat flux and entrainment as the main factors in the SST decrease in the Gulf of Guinea, while the latter are compensated in the MERCATOR run by a strong horizontal advection of SST (not shown). Thus, the residual term must essentially contain the horizontal and vertical diffusion effect, which is very important in this region for the heat budget in the mixed layer (Peter *et al.*, 2006), and maybe a consistent part of the vertical entrainment.

Linear regressions of these terms on the MERCATOR NCTI are presented in°C, showing their contribution to the evolution of the cold SST anomaly during 3 days (Figure 12). Clearly, the surface heat fluxes (Figure 12(c)) and entrainment (Figure 12(d)) do not contribute much to the evolution of the SST anomaly. On another hand, while the SST loses about 1°C in 6 days (between lag −6 and 0), the horizontal advection term is very large (Figure 12(b)) and dominated by the advection of the mean SST by anomalous surface currents $U'.\nabla\overline{T}$ (not shown). Current anomalies are indeed northward from lag −6 to 0 (Figure 12(b)) and result from the wind-stress anomaly, mainly meridional, in the presence of no or little Coriolis effect; they are maximal in the equatorial region between 1°S and 2°N to 4°N, to a first approximation because the mixed layer is shallower and the wind-stress stronger there (not shown). They transport northward colder water from the mean seasonal cold tongue spanning south of the Equator (see Figure 2) which cools the equatorial SST by almost 0.5°C in 6 days. The advection of anomalous SST by the mean currents also contributes significantly, albeit more weakly (by about 0.25°C, not shown); together, the two terms of horizontal advection explain more than half (almost two thirds) of the cold SSTA evolution at negative lags (Figure 12(b)). At lags 3 and 6, southward anomalous currents take place along the northern side of the Equator,

DOI: 10.1002/qj

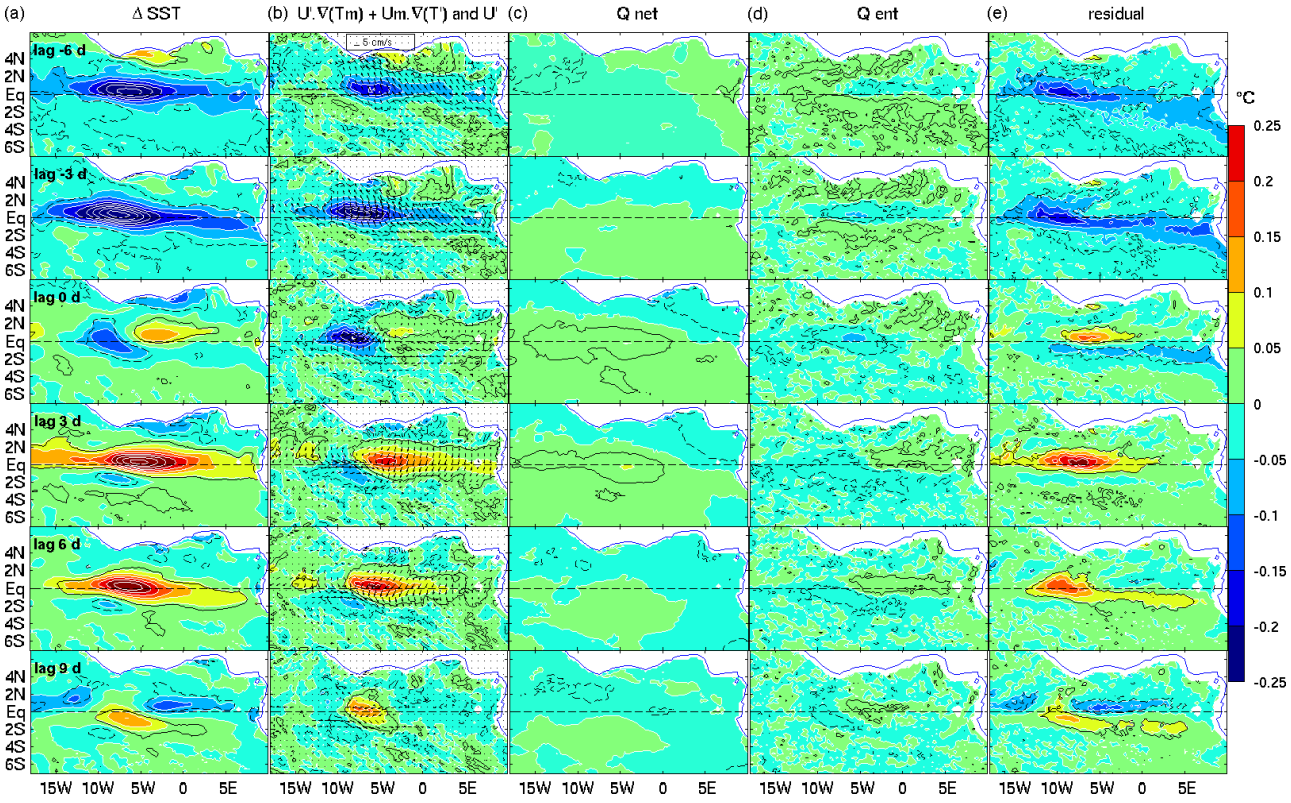

Figure 12. Linear lagged regressions of different contributions to the mixed-layer heat budget on the NCTI in the MERCATOR simulation, in °C per 3 days. The 10% significant correlation is plotted in black contour (plain for positive or dashed for negative). From left to right: (a) Δ SST, (b) $U'.\nabla\overline{T} + \overline{U}.\nabla T'$ with anomalous surface currents U', (c) net surface heat flux, (d) entrainment, and (e) residual. This figure is available in colour online at www.interscience.wiley.com/journal/qj

forced by the reversal of the wind anomalies. They bring back warmer water southward, increasing the temperature and leading to the warm SSTA in the 5°W–5°E northern equatorial band. Meanwhile, the westward displacement of the SST pattern observed in Figure 6 is well explained by advection with the mean currents: the cold SSTA just north of the Equator moves by about 6° westward from lags −6 to 9 (not shown), i.e. with a velocity of 40–50 cm.s^{-1} which is typical of the southern equatorial current between the Equator and 2°N in the model. The shift of the southern cold lobe in observations at lag 9 compared to the northern one would thus be due to the weaker westward mean surface currents around 2°S (Figure 6). As previously mentioned, the residual is probably composed in the first place of anomalous entrainment and diffusion, mainly vertical, and can be as important as the horizontal advection in the heat budget of the oceanic mixed layer (Figure 11(e), from lag 3 onwards).

Note that the surface flux data link together sections 5 and 6, since the ECMWF model assimilates TMI SST and QuikSCAT winds, and forces the MERCATOR simulation through surface heat fluxes and wind-stress; the argument in the last paragraph relies on the reversal of the MERCATOR NCTI-linked wind-stress which was expected and found in the regression of the ECMWF wind-stress (not shown), as in the QuikSCAT wind-stress regression (Figures 5 and 6). It was implicitly deduced from the orientation of the anomalous wind and currents that v' in MERCATOR was dominated by the Ekman component of surface current, i.e. by the direct response of the ocean surface. However, an indirect response could also take place through the geostrophic adjustment to the intensification of the SST front. In the Pacific cold tongue, at 2°N, 140°W, Cronin and Kessler (2009) indeed found a surprising mean near-surface shear primarily oriented to the left of the southeasterlies, due to the geostrophic contribution producing an Ekman transport toward the cold side of the front. Therefore, the ageostrophic shear balancing the wind stress could be much smaller than expected; in-depth investigations are needed to identify clearly the origin of the NCTI-correlated currents, Ekman and/or geostrophic. Moreover, a possible mixed gravity–Rossby wave could partly control v' east of 10°W (Athié and Marin, 2008; Han *et al.*, 2008) and, while controlled by the wind, contribute to amplifying the biweekly air–sea coupled signal. Eventually, the influence of the Bjerknes feedback needs to be investigated in this intraseasonal framework. Although it is weaker than in the Pacific (but stronger in boreal spring and summer than in other seasons), several recent studies confirmed its existence in the Atlantic (Keenlyside and Latif, 2007; Jansen *et al.*, 2009). However, because they used monthly data spanning several decades, they could not measure precisely the direct effect of the SST on zonal winds (i.e. at a daily timescale); the results presented here encourage the extension of the present analysis as far as the western equatorial Atlantic for evidences of this feedback.

DOI: 10.1002/qj

7. Summary

Air–sea interactions in the Gulf of Guinea during boreal spring and summer are analysed with high-quality satellite estimates of SST, surface wind-stress and precipitation. The results provide model-independent evidence of air–sea interaction and coupling, and an accurate OGCM simulation helps to understand the time evolution of the SST anomaly.

At intraseasonal time-scales, the highest EOF mode of SST variability during MAMJJA explains 16% of the total variance in the Gulf of Guinea and consists of a strong zonal anomaly straddling the Equator on the northern front of the cold tongue – where the MAMJJA mean SST gradient is the largest. The first mode of the surface wind-stress variability explains 20% of the total variance and corresponds to stronger or weaker southeasterlies over most of the Gulf of Guinea. Both modes are highly correlated at a few days lag, exhibiting a negative feedback and a strong periodicity of about two weeks. A regional negative feedback would explain up to one third of the biweekly variability in the Gulf of Guinea.

An SST index was built from the location of the most variant intraseasonal SST and used to describe the most variant linear air–sea interactions by performing lagged linear regressions of different anomalous fields. Stronger southeasterlies leading to a colder-than-normal SST in the EEA belong to a wide anticyclonic cell over the South Atlantic basin and explain about 10% of the NCTI variance. This is consistent with the observations of Caniaux *et al.* (2009) or Marin *et al.* (2009) who suggest that the 'wind bursts' leading to the cold equatorial SST in 2005 result from the variability of the St Helena anticyclone. No biweekly periodicity was clearly found in the NCTI-linked large-scale circulation, suggesting that this dominant variability observed in the Gulf of Guinea mainly comes from a regional negative feedback: a cold SSTA, initially forced by stronger winds than normal in the EEA, slows down in turn the trade winds after about one week, thereby creating a reverse wind anomaly.

This suggestion is supported by a closer view of the surface wind-stress and SST regression in the Gulf of Guinea which shows a remarkable agreement between the patterns of anomalous SST and wind-stress magnitude. This result is in agreement with the local MABL vertical redistribution mechanism which slows down the surface winds over a colder SST and increases them over a warm anomaly. Our analysis suggests that this SST-induced vertical effect is stronger than the SLP gradient effect induced by the SST gradient. However, the latter could be underestimated due to downwind thermal advection, which may geographically further the wind response to the SST anomaly. The anomalous strong monsoonal winds observed north of 2°N, concomitantly with the developing cold SST anomaly, could partly form this response. As they bring more rainfall and humidity along the southern coastal regions of West Africa, the continental SLP could feed back on these winds; it is an important issue for further investigations.

Through which mechanism the SST is modified by the wind-stress has been investigated with an OGCM forced by ECMWF surface fields. Surface heat fluxes do not seem to have a very significant contribution, except for the damping of the SSTA after its maximum. It was not possible to estimate with accuracy the impact of the mixing and entrainment, but their contributions are probably a major part of the heat budget (Peter *et al.*, 2006). However, the leading factor (by more than one half) was found to be the meridional advection of the mean SST by anomalous cross-equatorial currents forced by the anomalous meridional winds; at these short time-scales, horizontal advective cooling and warming respond faster and stronger than surface heat fluxes, entrainment and diffusion processes to the wind anomaly in the northern front of the cold tongue, because of the high meridional gradient of SST.

In summary, around the Equator, anomalous strong trade winds are followed by the cooling of the ocean surface within 5 days, mainly through the northward advection of the surface water in the cold tongue, and to a smaller extent through the anomalous vertical mixing and air–sea fluxes. Then, the cold SST anomaly visibly slows down the southeasterlies, thereby creating a reverse wind anomaly, which is maximal after 2 to 3 days. The mechanism involved in this retroaction is clearly linked to the vertical adjustment of the MABL stability, although the SLP gradient induced by the gradient of SST could also play an important role. These anomalous northerlies bring back warmer water from the north, resulting in the damping of the initial cold anomaly within 5 to 6 days. As the mean current advects the centre of the cold anomaly westward, a warm SST anomaly appears behind the cold anomaly along the Equator; it creates weak but significant anomalous southerlies, two weeks after the original wind burst, which may support a substantial part of the biweekly variability observed in the region. Further investigations are now needed to document the role of oceanic mixing processes, mainly the vertical diffusion and entrainment which appear to be as important as the horizontal advection.

Acknowledgements

We are thankful to Jean-Eudes Lombard and Gilles Garric for providing the MERCATOR simulation data, and to Harold F. Pierce for his help in retrieving the TRMM B42 rainfall data. This study was also supported by the AMMA project. Based on a French initiative, AMMA was built by an international scientific group and is currently funded by a large number of agencies, especially from France, United Kingdom, USA and Africa. It has been the beneficiary of a major financial contribution from the European Community's Sixth Framework Research Programme. Detailed information on scientific coordination and funding is available on the AMMA International website http://www.amma-international.org.

DOI: 10.1002/qj

The authors would like to thank Jerôme Sirven, Anne-Charlotte Peter, Denis Bourras, Alain Weill and particularly Frédéric Marin for many helpful discussions, as well as the three anonymous reviewers for their constructive remarks.

References

Athié G, Marin F. 2008. Cross-equatorial structure and temporal modulation of intraseasonal variability at the surface of the tropical Atlantic Ocean. *J. Geophys. Res.* **113**: C08020, DOI:10.1029/2007JC004332.

Back LE, Bretherton CS. 2009. On the relationship between SST gradients, boundary layer winds, and convergence over the tropical oceans. *J. Climate* **22**: 4182–4196.

Bunge L, Provost C, Lilly JM, D'Orgeville M, Kartavtseff A, Melice J-L. 2006. Variability of the horizontal velocity structure in the upper 1600 m of the water column on the Equator at 10°W. *J. Phys. Oceanogr.* **36**: 1287–1304.

Caniaux G, Giordani H, Redelsperger J-L, Guichard F, Key E, Wade M. 2009. Couplings between the Atlantic cold tongue, the St Helena anticyclone, and the African monsoon in boreal spring and summer. *J. Climate*, submitted.

Chang P. 1993. Seasonal cycle of sea surface temperature and mixed layer heat budget in the tropical Pacific Ocean. *Geophys. Res. Lett.* **20**: 2079–2082.

Chang P, Philander SGH. 1994. A coupled ocean–atmosphere instability of relevance to the seasonal cycle. *J. Atmos. Sci.* **51**: 3627–3648.

Chelton DB, Esbensen SK, Schlax MG, Thum N, Freilich MH, Wentz FJ, Gentemann CL, McPhaden MJ, Schopf PS. 2001. Observations of coupling between surface wind stress and sea surface temperature in the eastern tropical Pacific. *J. Climate* **14**: 1479–1498.

Chelton DB, Schlax MG, Freilich MH, Milliff RF. 2004. Satellite measurements reveal persistent small-scale features in ocean winds. *Science* **303**: 978–983.

Cronin MF, Kessler WS. 2009. Near-surface shear flow in the tropical Pacific cold tongue front. *J. Phys. Oceanogr.* **39**: 1200–1215.

Foltz GR, Grodsky SA, Carton JA, McPhaden MJ. 2003. Seasonal mixed layer heat budget of the tropical Atlantic Ocean. *J. Geophys. Res.* **108**: 3146, DOI:10.1029/2002JC001584.

Garric G, Bourdallé-Badie R, Le Galloudec O, Bricaud C, Derval C, Durand E, Drillet Y. 2008. '*Description of the interannual experiment ORCA025-T09, 1998–2006*.' Mercator Ocean Report, 235, Annexe 2.

Garzoli SL. 1987. Forced oscillations on the equatorial Atlantic basin during the Seasonal Response of the Equatorial Atlantic Program (1983–1984). *J. Geophys. Res.* **92**(C5): 5089–5100.

Gill AE. 1980. Some simple solutions for heat-induced tropical circulation. *Q. J. R. Meteorol. Soc.* **106**: 447–462.

Graham NE, Barnett TP. 1987. Sea surface temperature, surface wind divergence, and convection over tropical oceans. *Science* **238**: 657–659.

Grodsky SA, Carton JA. 2001. Coupled land/atmosphere interactions in the West African monsoon. *Geophys. Res. Lett.* **28**: 1503–1506.

Gu G, Adler RF. 2004. Seasonal evolution and variability associated with the West African monsoon system. *J. Climate* **17**: 3364–3377.

Guiavarc'h C, Treguier AM, Vangriesheim A. 2008. Remotely forced biweekly deep oscillations on the continental slope of the Gulf of Guinea. *J. Geophys. Res.* **113**: C06002, DOI:10.1029/2007JC004471.

Han W, Webster PJ, Lin J-L, Liu WT, Fu R, Yuan D, Hu A. 2008. Dynamics of intraseasonal sea level and thermocline variability in the equatorial Atlantic during 2002–03. *J. Phys. Oceanogr.* **38**: 945–967.

Hashizume H, Xie S-P, Fujiwara M, Shiotani M, Watanabe T, Tanimoto Y, Liu WT, Takeuchi K. 2002. Direct observations of atmospheric boundary layer response to SST variations associated with tropical instability waves over the eastern equatorial Pacific. *J. Climate* **15**: 3379–3393.

Hayes SP, McPhaden MJ, Wallace JM. 1989. The influence of sea-surface temperature on surface wind in the eastern equatorial Pacific: Weekly to monthly variability. *J. Climate* **2**: 1500–1506.

Houghton RW, Colin C. 1987. Wind-driven meridional eddy heat flux in the Gulf of Guinea. *J. Geophys. Res.* **92**(C10): 10777–10786.

Hsu SA. 1984. Sea-breeze-like winds across the north wall of the Gulf Stream: An analytical model. *J. Geophys. Res.* **89**(C2): 2025–2028.

Huffman GJ, Adler RF, Morrissey MM, Bolvin DT, Curtis S, Joyce R, McGavock B, Susskind J. 2001. Global precipitation at one-degree daily resolution from multisatellite observations. *J. Hydrometeorol.* **2**: 36–50.

Jansen MF, Dommenget D, Keenlyside N. 2009. Tropical atmosphere–ocean interactions in a conceptual framework. *J. Climate* **22**: 550–567.

Jochum M, Cronin MF, Kessler WS, Shea D. 2007. Observed horizontal temperature advection by tropical instability waves. *Geophys. Res. Lett.* **34**: L09604, DOI:10.1029/2007GL029416.

Keenlyside NS, Latif M. 2007. Understanding equatorial Atlantic interannual variability. *J. Climate* **20**: 131–142.

Klein SA, Hartmann DL. 1993. The seasonal cycle of low stratiform clouds. *J. Climate* **6**: 1587–1606.

Kouadio YK, Ochou DA, Servain J. 2003. Tropical Atlantic and rainfall variability in Côte Ivoire. *Geophys. Res. Lett.* **30**: 8005, DOI:10.1029/2002GL015290.

Kubota M, Kano A, Muramatsu H, Tomita H. 2003. Intercomparison of various surface latent heat flux fields. *J. Climate* **16**: 670–678.

Lamb PJ. 1978a. Large-scale tropical Atlantic surface circulation patterns associated with Subsaharan weather anomalies. *Tellus* **30**: 240–251.

Lamb PJ. 1978b. Case studies of tropical Atlantic surface circulation patterns during recent sub-Saharan weather anomalies: 1967 and 1968. *Mon. Weather Rev.* **106**: 482–491.

Large WG, Pond S. 1981. Open ocean momentum flux measurements in moderate to strong winds. *J. Phys. Oceanogr.* **11**: 324–336.

Large WG, McWilliams JC, Doney SC. 1994. Oceanic vertical mixing: A review and a model with a nonlocal boundary layer parameterization. *Rev. Geophys.* **32**: 363–403.

Li T, Philander SGH. 1997. On the seasonal cycle of the equatorial Atlantic Ocean. *J. Climate* **10**: 813–817.

Lindzen RS, Nigam S. 1987. On the role of sea surface temperature gradients in forcing low-level winds and convergence in the Tropics. *J. Atmos. Sci.* **44**: 2418–2436.

Liu TW, Xie X, Polito PS, Xie S-P, Hashizume H. 2000. Atmospheric manifestation of tropical instability wave observed by QuikSCAT and Tropical Rain Measuring Mission. *Geophys. Res. Lett.* **27**: 2545–2548.

Marin F, Caniaux G, Bourlès B, Giordani H, Gouriou Y, Key E. 2009. Why were sea surface temperatures so different in the eastern equatorial Atlantic in June 2005 and 2006? *J. Phys. Oceanogr.* **39**: 1416–1431.

Mitchell TP, Wallace JM. 1992. The annual cycle in equatorial convection and sea surface temperature. *J. Climate* **5**: 1140–1156.

Mounier F, Janicot S, Kiladis GN. 2008. The West African monsoon dynamics. Part III: The quasi-biweekly zonal dipole. *J. Climate* **21**: 1911–1928.

Neelin JD. 1989. On the interpretation of the Gill model. *J. Atmos. Sci.* **46**: 2466–2468.

Norris JR. 1998. Low cloud type over the ocean from surface observations. Part II: Geographical and seasonal variations. *J. Climate* **11**: 383–403.

Okumura Y, Xie S-P. 2004. Interaction of the Atlantic equatorial cold tongue and the African monsoon. *J. Climate* **17**: 3589–3602.

O'Neill LW, Chelton DB, Esbensen SK. 2003. Observations of SST-induced perturbations of the wind stress field over the Southern Ocean on seasonal timescales. *J. Climate* **16**: 2340–2354.

Opoku-Ankomah Y, Cordery I. 1994. Atlantic sea surface temperatures and rainfall variability in Ghana. *J. Climate* **7**: 551–558.

Peter A-C, Le Hénaff M, du Penhoat Y, Menkes CE, Marin F, Vialard J, Caniaux G, Lazar A. 2006. A model study of the seasonal mixed layer heat budget in the equatorial Atlantic. *J. Geophys. Res.* **111**: C06014, DOI:10.1029/2005JC003157.

Samelson RM, Skyllingstad ED, Chelton DB, Esbensen SK, O'Neill LW, Thum N. 2006. On the coupling of wind stress and sea surface temperature. *J. Climate* **19**: 1557–1566.

Small RJ, Xie S-P, Hafner J. 2005. Satellite observations of mesoscale ocean features and copropagating atmospheric surface fields in the tropical belt. *J. Geophys. Res.* **110**: C02021, DOI:10.1029/2004JC002598.

Small RJ, de Szoeke SP, Xie S-P, O'Neill L, Seo H, Song Q, Cornillon P, Spall M, Minobe S. 2008. Air–sea interaction over ocean fronts and eddies. *Dyn. Atmos. Oceans* **45**: 274–319.

Sultan B, Janicot S. 2003. The West African monsoon dynamics. Part II: The 'preonset' and 'onset' of the summer monsoon. *J. Climate* **16**: 3407–3427.

Sweet W, Fett R, Kerling J, La Violette P. 1981. Air–sea interaction effects in the lower troposphere across the north wall of the Gulf Stream. *Mon. Weather Rev*. **109**: 1042–1052.

Von Storch H, Zwiers FW. 1999. *Statistical analysis in climate research*. Cambridge University Press.

Wai MM-K, Stage SA. 1989. Dynamical analyses of marine atmospheric boundary layer structure near the Gulf Stream oceanic front. *Q. J. R. Meteorol. Soc.* **115**: 29–44.

Waliser DE, Graham NE Gautier C. 1993. Comparison of the highly reflective cloud and outgoing longwave radiation datasets for use in estimating tropical deep convection. *J. Climate* **6**: 331–353.

Wallace JM, Mitchell TP, Deser C. 1989. The influence of sea-surface temperature on surface wind in the eastern equatorial Pacific: Seasonal and interannual variability. *J. Climate* **2**: 1492–1499.

Xie S-P. 2004. Satellite observations of cool ocean–atmosphere interaction. *Bull. Am. Meteorol. Soc.* **85**: 195–208.

Xie S-P, Philander SGH. 1994. A coupled ocean–atmosphere model of relevance to the ITCZ in the eastern Pacific. *Tellus* **46A**: 340–350.

Young JA. 1987. Boundary layer dynamics of tropical and monsoonal flows. Pp 461–500 in *Monsoon meteorology*. Oxford University Press.

Yu L, Jin X, Weller RA. 2008. '*Multidecade global flux datasets from the Objectively Analyzed air–sea Fluxes (OAFlux) project: Latent and sensible heat fluxes, evaporation, and related surface meteorological variables*.' Woods Hole Oceanographic Institution, OAFlux Project Technical Report, OA-2008-01, 64 pp. Woods Hole, Massachusetts, USA.

DOI: 10.1002/qj